RESEARCH PAPER

Channels 6:4, 197-205; July/August 2012; © 2012 Landes Bioscience

Structural determinants of $Ca_V1.3$ L-type calcium channel gating

Andreas Lieb, Anja Scharinger, Simone B. Sartori, Martina J. Sinnegger-Brauns and Jörg Striessnig*

Pharmacology and Toxicology; Institute of Pharmacy and Center for Molecular Biosciences; University of Innsbruck; Innsbruck, Austria

Keywords: cacna1d, $Ca_v1.3$, voltage-gated Ca^{2+} channels, species differences, gating, mutagenesis

Abbreviations: aa, amino acid; CDI, calcium dependent inactivation; CTM, C-terminal modulatory domain; LTCC, L-type calcium channel; Po, open probability; scg, superior cervical ganglion; $V_{0.5}$, voltage of half maximal activation

A C-terminal modulatory domain (CTM) tightly regulates the biophysical properties of $Ca_v1.3$ L-type Ca^{2+} channels, in particular the voltage dependence of activation ($V_{0.5}$) and Ca^{2+} dependent inactivation (CDI). A functional CTM is present in the long C-terminus of human and mouse $Ca_v1.3$ ($Ca_v1.3_L$), but not in a rat long cDNA clone isolated from superior cervical ganglia neurons ($rCa_v1.3_{scg}$). We therefore addressed the question if this represents a species-difference and compared the biophysical properties of $rCa_v1.3_{scg}$ with a rat cDNA isolated from rat pancreas ($rCa_v1.3_L$).

When expressed in tsA-201 cells under identical experimental conditions $rCa_v1.3_L$ exhibited Ca^{2+} current properties indistinguishable from human and mouse $Ca_v1.3_L$, compatible with the presence of a functional CTM. In contrast, $rCa_v1.3_{scg}$ showed gating properties similar to human short splice variants lacking a CTM. $rCa_v1.3_{scg}$ differs from $rCa_v1.3_L$ at three single amino acid (aa) positions, one alternative spliced exon (exon31), and a N-terminal polymethionine stretch with two additional lysines. Two aa (S244, A2075) in $rCa_v1.3_{scg}$ explained most of the functional differences to $rCa_v1.3_L$. Their mutation to the corresponding residues in $rCa_v1.3_L$ (G244, V2075) revealed that both contributed to the more negative $V_{0.5}$, but caused opposite effects on CDI. A2075 (located within a region forming the CTM) additionally permitted higher channel open probability. The cooperative action in the double-mutant restored gating properties similar to $rCa_v1.3_L$. We found no evidence for transcripts containing one of the single $rCa_v1.3_{scg}$ mutations in rat superior cervical ganglion preparations. However, the $rCa_v1.3_{scg}$ variant provided interesting insight into the structural machinery involved in $Ca_v1.3$ gating.

Introduction

Voltage-gated $Ca_v1.3$ Ca^{2+} channels represent a member of the dihydropyridine-sensitive class of L-type Ca^{2+} channels (LTCCs). Together with $Ca_v1.2$ LTCCs they are expressed in mammalian electrically excitable tissues. $Ca_v1.3$ knockout mice[1-3] and a recently discovered human disease (Sinoatrial Node Dysfunction and Deafness, SANDD) [4] revealed a key role of these channels for hearing, cardiac pacemaker function and neuronal excitability. $Ca_v1.3$ channels possess unique gating properties that privilege them to carry Ca^{2+} inward currents at threshold potentials in sinoatrial node cells,[2] chromaffin cells[5] neurons as well as within the operating range of cochlear inner hair cells.[6,7] These gating properties are tightly controlled by a C-terminal modulatory domain (CTM) with strong effects on $Ca_v1.3$ activation and inactivation gating behavior as well as open probability (Po).[8-10] The CTM is formed by an intermolecular protein-protein interaction of a distal (DCRD) with a proximal C-terminal modulatory domain (PCRD), thereby decreasing the calmodulin affinity for the channel.[11,12] Alternative splicing within the $Ca_v1.3$ C-terminus is tissue-specific and involves structural motifs required for high affinity interaction with calmodulin and the proper function of the CTM. Since calmodulin serves as the Ca^{2+} sensor for autoinhibitory Ca^{2+}-dependent inactivation (CDI) of voltage-gated Ca^{2+} channels, splicing causes pronounced gating differences between long and short $Ca_v1.3$.[8,9,11,13,14] Short CTM-deficient splice variants have higher Po, activate at more negative voltages and show accelerated CDI than full length variants with a functional CTM ($Ca_v1.3_L$).[8,9] This modulatory domain has been extensively characterized with cDNA constructs cloned from human pancreas,[8,9] and its effects were also reproduced with short and long mouse constructs (unpublished observations). In contrast, the modulation was not reported for $Ca_v1.3$ channels cloned from rat superior cervical ganglia neurons (scg) (termed $rCa_v1.3_{scg}$).[15] Despite the presence of a full length C-terminal tail, $rCa_v1.3_{scg}$ showed gating properties similar to those observed in short splice variants,[11,15-20] suggesting a dysfunctional CTM. It is at present unclear if this could represent a significant species difference in $Ca_v1.3$ channel modulation and to which extent transcripts corresponding to $rCa_v1.3_{scg}$ are expressed in rat scg (and perhaps other tissues). Despite considerable use of $rCa_v1.3_{scg}$ constructs in $Ca_v1.3$ research[11,13-18] it has never been tested if

*Correspondence to: Jörg Striessnig; Email: joerg.striessnig@uibk.ac.at
Submitted: 05/25/12; Revised: 06/04/12; Accepted: 06/04/12
http://dx.doi.org/10.4161/chan.21002

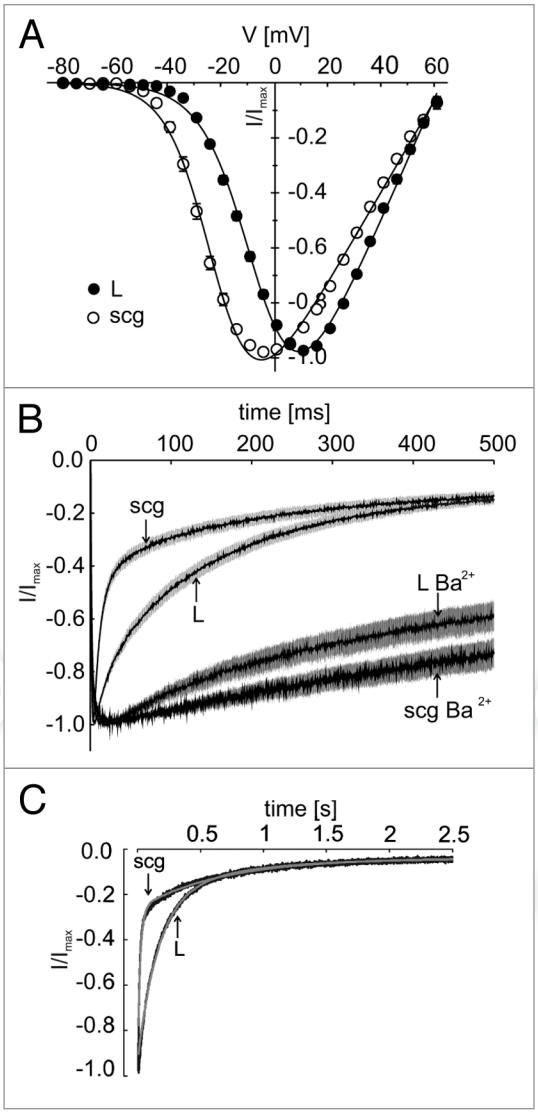

Figure 1. Gating differences between $rCa_v1.3_{scg}$ and $rCa_v1.3_L$. (A) Normalized voltage activation range of $rCa_v1.3_{scg}$ (○) and $rCa_v1.3_L$ (●). Activation parameters are given in Table 1. Data points are means ± SE. Error bars are often smaller than symbol size. (B) Inactivation of I_{Ca} (scg, L) and I_{Ba} (L Ba^{2+}, scg Ba^{2+}) of $rCa_v1.3_{scg}$ and $rCa_v1.3_L$ during the first 500 ms of a 2.5 sec test pulse to V_{max}. Inactivation parameters obtained by fitting the data to a double exponential function are given in **Table 2**. Data are shown as means (black line) with SE (gray). (C) Representative experiments, described in (B) and corresponding fits are illustrated.

corresponding transcripts indeed exist. Moreover, the molecular determinants responsible for the observed functional differences between $rCa_v1.3_{scg}$ and other rat and mammalian $Ca_v1.3_L$ α_1-subunits have never been systematically analyzed although they could provide novel information about structural features controlling channel gating. Here we provide bioinformatic and biochemical evidence that $rCa_v1.3_{scg}$ transcripts are indeed not expressed at detectable levels in rat scg and should therefore not be considered to be contributing to $Ca_v1.3$ functional diversity. We took advantage of the minor aa differences between $rCa_v1.3_{scg}$ and the long rat $Ca_v1.3$ α_1-subunit ($rCa_v1.3_L$) predicted from the rat cacna1d gene. This allowed us to identify these residues as those responsible for the abnormal gating behavior of $rCa_v1.3_{scg}$ and as key elements in $Ca_v1.3$ Ca^{2+} channel gating.

Results

Major gating differences between $rCa_v1.3_L$ and $rCa_v1.3_{scg}$. We have recently discovered that an intramolecular protein interaction within the C-terminus of long $Ca_v1.3$ α_1-subunit splice variants forms CTM that stabilizes a gating mode with activation at a more positive voltage range, slower CDI and lower Po. When analyzed under identical experimental conditions after expression in tsA-201 cells, we found that this regulation is present in the long variant of human $Ca_v1.3$ ($Ca_v1.3_L$) [9] and the common rat $rCa_v1.3$ α_1-subunit originally isolated from rat pancreas (termed $rCa_v1.3_L$ in analogy to the human $Ca_v1.3_L$ containing a full length C-terminal tail[8]) but not in the corresponding long rat $rCa_v1.3$ variant isolated from scg ($rCa_v1.3_{scg}$). The activation threshold and $V_{0.5}$ of $rCa_v1.3_{scg}$ was about 16 mV more negative (**Fig. 1A and Table 1**) and the inactivation time course of Ca^{2+} currents (I_{Ca}) was significantly faster than for $rCa_v1.3_L$ (**Fig. 1B and Table 2**) and human $Ca_v1.3_L$ (not shown, cf. 8 and 9). Faster inactivation was due to enhanced CDI as evident from the even slower inactivation when equimolar Ba^{2+} served as the charge carrier (I_{Ba}, **Fig. 1B**). This finding indicates potential species differences or the existence of a scg-specific $Ca_v1.3$ splice variant. We therefore investigated the expression of the $rCa_v1.3_{scg}$ variant in rat scg.

$rCa_v1.3_{scg}$ transcripts were not detected in rat scg RNA preparations. Comparison of the aa sequence of the $rCa_v1.3_{scg}$ α_1 construct with the canonical rat $Ca_v1.3_L$ α_1 sequence revealed only minor structural differences (**Fig. 2A**). Single aa exchanges were found in positions 244 (S in $rCa_v1.3_{scg}$, G in $rCa_v1.3_L$), 1104 (V to A) and 2075 (A to V), an alternatively spliced locus (exon 31 in $rCa_v1.3_{scg}$ vs. exon 31A in $rCa_v1.3_L$) also found in mouse and human,[21] and a polymethionine stretch with two additional lysines at the N-terminus (7M2K), which is present in the mRNA of different species but was absent in the $rCa_v1.3_{scg}$ construct.[15] Inspection of the rat genomic cacna1d-sequence (GenBank accession number NW_047469.2) revealed the DNA sequence previously reported for $rCa_v1.3_L$ α_1-subunits, isolated from pancreas (D38101, D38102), brain (M57682) and kidney (M99221). We found no genomic evidence for any of the single amino acid differences reported for $rCa_v1.3_{scg}$. The residues concerned are also highly conserved in other species, such as human (EU363339.1), mouse (NP_001077085), cattle (NP_001179954) and rabbit (XP_002713437), with no evidence for variation as found in $rCa_v1.3_{scg}$. Since the three single aa differences S244G, V1104A, A2075V had been detected in scg preparations[15] but not in rat brain,[22] we re-evaluated the abundance of these variants in Sprague-Dawley scg preparations, by using a transcript-scanning approach. $rCa_v1.3_L$ and $rCa_v1.3_{scg}$-specific sequences were determined by restriction enzyme profiling of cloned PCR products. Neither S244 (n = 122) nor V1104 (n = 106) or A2075 (n = 109) could be detected (they would appear as undigested PCR products in lanes b, and digested PCR products in lanes c in **Fig. 2B**) in more than hundred clones analyzed for each position.

Table 1. Biophysical properties of $rCa_v1.3$ α_1-subunit mutations

$Ca_v1.3$ construct	$V_{0.5}$	act tresh	k_{act}	V_{rev}	n
$rCa_v1.3_{scg}$	-21.34 ± 0.98	-50.30 ± 0.89	8.51 ± 0.30	63.38 ± 1.07	23
$rCa_v1.3_L$	-5.19 ± 0.73^{aaa}	-39.43 ± 0.51^{aaa}	9.10 ± 0.12	65.37 ± 0.62	55
$rCa_v1.3_{scg}$ construct					
7M2K	-22.51 ± 1.45	-48.87 ± 1.53	7.43 ± 0.28^{a}	65.78 ± 1.38	11
S244G	-18.29 ± 1.14	-44.27 ± 1.10^{aaa}	7.37 ± 0.30^{a}	61.25 ± 1.75	12
V1104A	-22.98 ± 1.59	-50.14 ± 0.67	7.63 ± 0.29	65.40 ± 1.39	9
A2075V	-15.49 ± 0.76^{aaa}	-48.22 ± 0.76	9.09 ± 0.11	64.60 ± 0.67	31
S244G/A2075V	-11.20 ± 0.78^{bbb}	-43.47 ± 0.64^{bbb}	8.86 ± 0.17	65.22 ± 1.15	30
V1104A/A2075V	-14.00 ± 1.29	-47.51 ± 1.00	9.05 ± 0.26	65.25 ± 1.53	7
7M2K/S244G/A2075V	-11.66 ± 0.91	-44.15 ± 1.39	8.88 ± 0.24	62.87 ± 0.88	11
S244G/V1104A/A2075V	-10.23 ± 0.88	-42.59 ± 0.89	8.75 ± 0.27	63.93 ± 1.14	12
S244G/V1104A/ex31A/A2075V	-8.87 ± 0.87	-40.99 ± 0.63	8.70 ± 0.15	64.21 ± 0.78	14
7M2KS244G/V1104A/ex31A/A2075V	-5.66 ± 0.99^{ccc}	-37.10 ± 0.92^{ccc}	7.94 ± 0.31	69.29 ± 0.77	11

Parameters (means ± S.E.) were obtained by fitting data of I–V relationships as described in methods; statistical significances are indicated for comparisons vs. $rCa_v1.3_{scg}$ (a–aaa), vs. A2075V (b–bbb) and vs. S244G/A2075V (c, mL, ccc) (one-way Anova with Bonferroni post-test).

This suggests minimal or no $rCa_v1.3_{scg}$ expression in adult rat scg. Direct sequencing of PCR products amplified from two independent reverse transcriptions also revealed no evidence for low abundance DNA sequence variations in the codons concerned (**Fig. 2C**). Therefore our data do not confirm the expression of $rCa_v1.3_{scg}$-specific sequences in scg.

As shown above we found profound functional differences between $rCa_v1.3_{scg}$ and $rCa_v1.3_L$. Therefore the observed aa differences provided us with a unique opportunity to study their role for $Ca_v1.3$ channel function.

Impact of single and combined mutations on $rCa_v1.3_{scg}$ gating. To reveal the contribution of these minor structural differences for channel gating we first converted the single aa exchanges individually (S244G, V1104A, A2075V) and in combination to $rCa_v1.3_L$ residues within the $rCa_v1.3_{scg}$ backbone and tested to which extent this resulted in restoration of $rCa_v1.3_L$ functional properties. We also analyzed the alternatively spliced locus (exon 31/exon 31A) and the N-terminal polymethionine stretch with two additional lysines (7M2K). S244 in $rCa_v1.3_{scg}$ is located at the cytoplasmatic end of segment S4, which forms part of the voltage sensing domain in repeat I (**Fig. 2A**). Conversion of S244 to the corresponding glycine in $rCa_v1.3_L$ (S244G) shifted the activation threshold (by 6.03 ± 1.47 mV, $p < 0.001$) and $V_{0.5}$ (3.06 ± 1.59 mV) to more positive voltages (**Fig. 3A and Table 1**). It also induced a significant decrease in k_{act} (**Table 1**). S244G enhanced inactivation of I_{Ca} during depolarizations to test potentials over a broad voltage range (**Fig. 3B and Table 2**). Since no increase in inactivation was observed for I_{Ba} (**Fig. 3B**) this enhancement reflected accelerated CDI. Faster inactivation resulted from a significant decrease of the time constant of the fast inactivating component (τ_{fast}) and a significant increase in its contribution to inactivation (**Fig. 4 and Table 2**). As an estimate for changes in channel Po we compared the relative size of ON gating currents (Q_{on}) with tail current amplitude (I_{tail}). This ratio was similar for $rCa_v1.3_{scg}$ and S244G suggesting that the mutation did not change Po (**Fig. 5**). Taken together, mutation S244G in $rCa_v1.3_{scg}$ partially restores the more positive activation threshold of $rCa_v1.3_L$ but accelerates CDI. Among a large number of point mutations previously studied,[23,24] S244G is to our knowledge the first mutation capable of significantly enhancing CDI. This finding was surprising because the mutation was expected to reduce CDI to the more moderate level observed in $rCa_v1.3_L$.

In contrast to S244G, reverting A2075 in $rCa_v1.3_{scg}$ to the corresponding valine in $rCa_v1.3_L$ (A2075V) inhibited CDI (**Figs. 3B and 4**). Quantification over a large voltage range revealed that CDI was strongly decreased and even significantly slower than in $rCa_v1.3_L$ (see F-values in **Fig. 3B**). Voltage-dependent inactivation (i.e., inactivation kinetics of I_{Ba}, VDI) was not affected (**Fig. 3B**). Slowing of CDI by the A2075V mutation resulted in a significant about 8-fold increase in τ_{fast} and a 22% decrease of the contribution of the fast component (**Fig. 4 and Table 2**). Like S244G, A2075V also caused a partial but significant shift of $V_{0.5}$ to more positive voltages by about 6 mV (**Fig. 3A and Table 1**). These data show that although both single mutations shift the channel's activation voltage range to more positive voltages, they exert opposite effects on CDI. Also in contrast to S244G, A2075V increased Q_{on} relative to I_{tail} (**Fig. 5**) suggesting a decrease in Po. Mutation of V1104 in $rCa_v1.3_{scg}$ to alanine, or inclusion of the 7M2K sequence at the N-terminus (**Tables 1 and 2**) caused no significant effects on $V_{0.5}$, activation thresholds and on current kinetics. We therefore hypothesized that the combined mutation of S244G and A2075V in $rCa_v1.3_{scg}$ restores most of the gating properties of $rCa_v1.3_L$. In the double mutant S244G/A2075V CDI parameters were restored to values indistinguishable from those of $rCa_v1.3_L$ (**Figs. 3 and 4**). This was again verified over a broad voltage range showing that F-values of S244G/A2075V and $rCa_v1.3_L$ were not significantly different (**Fig. 3B**). VDI was also not affected by the double mutation (**Fig. 3B**). Introduction of V1104A into A2075V (V1104A/A2075V) was without noticeable effect on gating parameters (**Tables 1 and 2**).

The double mutation S244G/A2075V robustly shifted $V_{0.5}$ by about 10 mV to more positive voltages, thus representing

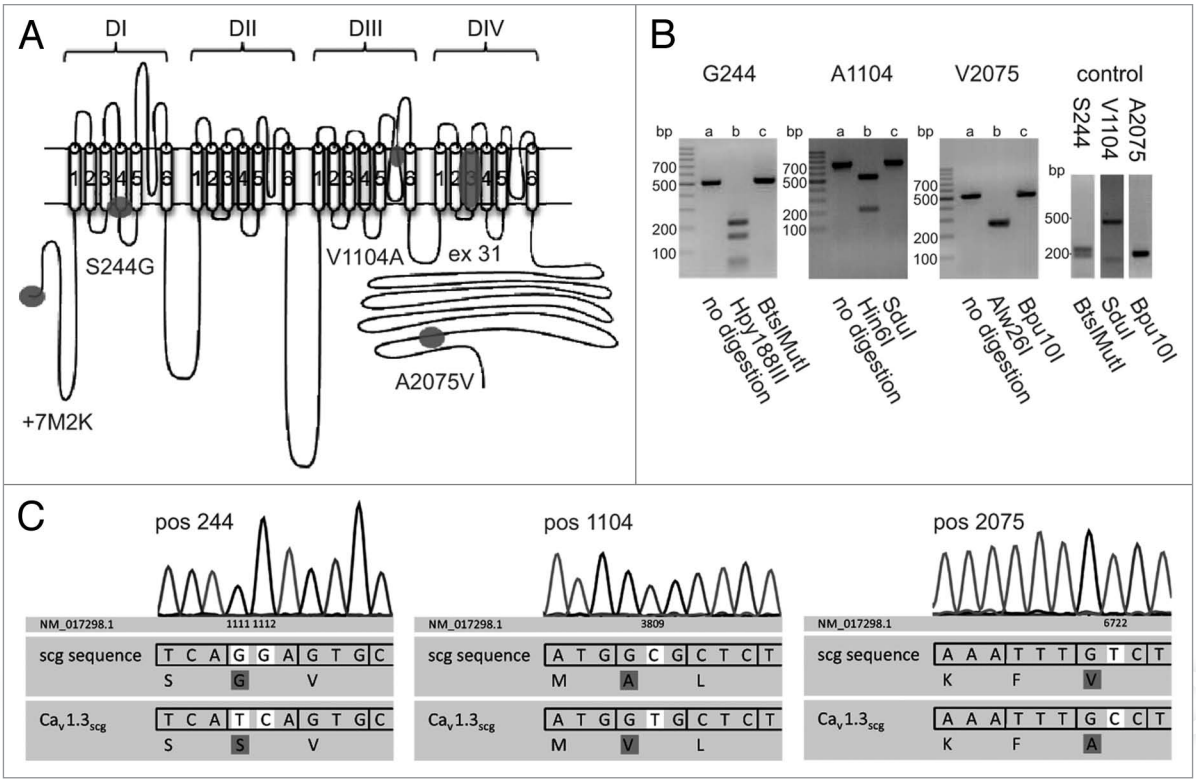

Figure 2. Structural differences between $rCa_v1.3_{scg}$ and $rCa_v1.3_L$ and tissue expression. (A) Scheme of $Ca_v1.3$ α1-subunits showing the approximate positions of structural differences (highlighted in gray) between $rCa_v1.3_L$ and $Ca_v1.3_{scg}$ as described in the text. (B) Restriction enzyme mapping of amino acid positions (pos) 244, 1104 and 2075; representative agarose gel separations of digests are shown. PCR products of regions of interest were amplified from rat scg cDNA, cloned and analyzed by colony PCR. Lanes a, undigested PCR products; lanes b, PCR products treated with enzymes only digesting DNA sequence reporting amino acid residues G244 (Hyp188III, n = 122 clones analyzed), A1104 (Hin6I, n = 106), or V2075 (Alw26I, n = 109); lanes c, control treatment with enzymes specifically digesting PCR products containing sequence for S244 (BtsIMutI, n = 16), V1104 (SduI, n = 13) or A2075 (Bpu10I, n = 14). For the latter enzymes positive control digests of PCR products amplified using $rCa_v1.3_{scg}$ cDNA plasmids as a template are also shown. Note that differences in fragment size between sample and controls arise from use of different primer positions (see methods). (C) Results of direct sequencing of PCR products containing the reported nucleotide exchange. Nucleotide numbers are given according to the reference sequence (NM_017298.1). The nucleotide and corresponding amino acid sequence of the PCR products amplified from rat superior cervical ganglion cDNA (scg sequence) are shown in comparison with the respective $rCa_v1.3_{scg}$ sequence below. The critical nucleotide and resulting amino acid differences are highlighted. No additional low abundance nucleotide sequences could be detected, arguing against the presence of detectable amounts of $rCa_v1.3_{scg}$ transcripts.

an additive effect of the two individual mutations (**Table 1**). However, it still activated at about 6 mV more negative voltages than $rCa_v1.3_L$ (**Fig. 3A and Table 1**). To further determine the structural basis of this remaining difference we constructed a variety of combined mutations. Inclusion of V1104 and exon31A in S244G/A2075V neither alone nor in combination restored the $V_{0.5}$ of $rCa_v1.3_L$ (**Table 1**). However, the additional insertion of the $rCa_v1.3_L$ N-terminal peptide 7M2K (that completely restored the sequence of $rCa_v1.3_L$ although in a different expression plasmid[25]), restored the voltage activation range of $rCa_v1.3_L$ as expected. This indicates a complex cooperative interaction between 7M2K, exon31 and A1104 for control of activation gating.

Discussion

The recent discovery of a C-terminal modulatory domain within the long C-terminal tail of LTCCs provided a fresh perspective on how these channels undergo automodulatory fine tuning through C-terminal intramolecular protein-protein interaction. In $Ca_v1.4$ α_1-subunits this interaction can completely suppress CDI. This stabilizes very slow inactivation of Ca^{2+} currents as required for continuous $Ca_v1.4$ channel activity in retinal photoreceptor terminals.[26-28] In $Ca_v1.2$ this modulatory domain serves as the structural framework to enable its regulation by cAMP-dependent protein kinase during the flight-and fight response.[29,30] $Ca_v1.3$ variants with full-length or truncated C-termini show pronounced differences in gating behavior that affect $Ca_v1.3$-mediated Ca^{2+} entry during physiological neuron-like firing patterns.[8] Therefore the isolation of rat scg $Ca_v1.3$ channel transcripts ($rCa_v1.3_{scg}$, GenBank accession numbers: AF370010, AF370009) containing specific single amino acid differences and completely lacking this regulatory capacity[11,15] implied a puzzling species difference. As the exchanges are not predicted by the genomic cacna1d sequence (GenBank accession number: NW_047469.2), they could result from nuclear pre-mRNA editing by adenosine

deaminases (ADARs). This is the most abundant type of RNA editing found in higher eukaryotes and has been reported for $Ca_v1.3$ α_1-subunits.[10,31] It results in a post-transcriptional single nucleotide change from adenosine to inosine, which is interpreted as guanosine by the translation machinery. As evident from **Figure 2C**, however, this mechanism cannot explain the single amino acid changes in $rCa_v1.3_{scg}$. Our PCR analysis of reverse transcribed RNA samples from rat scg could not detect the single amino acid differences specifically reported for $rCa_v1.3_{scg}$ (GenBank accession numbers: AF370010, AF370009). We therefore conclude that, if $rCa_v1.3_{scg}$ transcripts exist at all, they are of very low abundance. However, we cannot rule out the possibility that $rCa_v1.3_{scg}$ is the result of molecular processing not yet described for $Ca_v1.3$ α_1-subunits (such as utilization of microexons[32]) that occurs conditionally (e.g., in an age or health state-dependent manner) and has thus evaded our analysis.

We show that the long $rCa_v1.3$ α_1-subunit splice variant isolated from rat pancreas exhibits gating properties indistinguishable from those cloned from human and mouse. We found that the mutation of two aa residues in $rCa_v1.3_{scg}$ to $rCa_v1.3_L$ sequence also restored most of the gating properties of $rCa_v1.3_L$. Both mutations additively contributed in shifting $V_{0.5}$ to more positive voltages. However, their effects on CDI were more complex. Whereas S244G enhanced CDI beyond inactivation of $rCa_v1.3_{scg}$, A2075V caused a strong reduction of CDI that was even slower than for $rCa_v1.3_L$. These opposite effects eventually led to inactivation of S244G/A2075V very similar to rat and human $Ca_v1.3_L$. These data also suggest that $Ca_v1.3$ constructs containing either serine in position 244 or alanine in position 2075, but not both, would display unusual biophysical properties different from all other $Ca_v1.3$ splice variants described so far. However, the presence of both induced gating properties very similar to human and mouse short $Ca_v1.3$.

The cytoplasmic side of the S4 transmembrane voltage-sensor helices transmits voltage-dependent movements to their S4-S5 linkers which make contacts to the pore-forming S6 helices and thereby participate in channel opening and closing.[33] Accordingly, mutations in this region affect channel gating as, for example, seen in mutations associated with human diseases. Mutation S229P in $Ca_v1.4$ (causing CSNB2) completely prevents channel opening[34] and S218L in $Ca_v2.1$ (causing Familial Hemiplegic Migraine Type I) causes a strong negative shift in $V_{0.5}$ and a slowing of VDI.[35] It is unknown how S244G could enhance CDI even beyond the fast CDI already seen in $rCa_v1.3_{scg}$. In addition, how can we explain the observation that mutations S244G and A2075V both cause a similar positive shift of $V_{0.5}$ but show opposite effects on CDI? One possible unifying interpretation is based on a recent model assuming an allosteric CDI mechanism[24] in which inactivation represents an allosteric modulation of channel opening. It assumes that channels can adopt either a normal gating mode or an "inactivated" mode in which their opening is allosterically inhibited but not completely prevented by interaction with calmodulin. In this model mutations that promote opening would also enhance opening of the inactivated mode and therefore diminish CDI_{max} (i.e., CDI observed when all channels are in the inactivated mode). Conversely, mutations

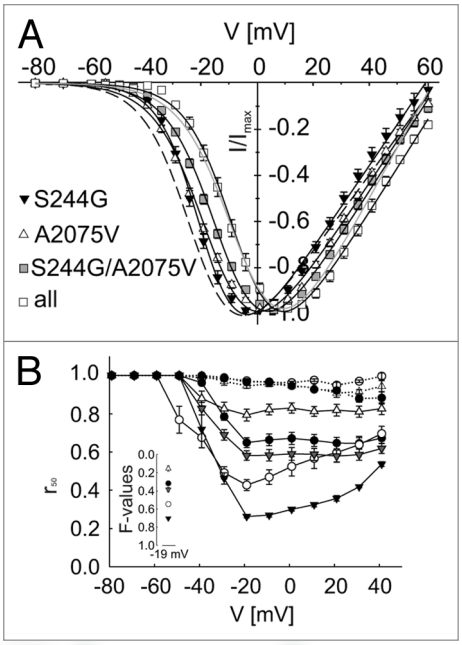

Figure 3. Voltage-dependent activation of $rCa_v1.3_{scg}$ mutants. (A) Normalized I-V relationships of $rCa_v1.3_{scg}$ mutations S244G (▼), A2075V (△), double mutation S244G/A2075V (■), and "all" amino acid exchanges (resulting in $rCa_v1.3_L$ sequence in the $rCa_v1.3_{scg}$ plasmid) (□). Lines represent best fits to the equation described in methods, parameters are given in **Table 1**. I - V curves for $rCa_v1.3_L$ (gray), and $rCa_v1.3_{scg}$ (broken line) are shown for comparison (taken from Fig. 1A). (B) Voltage dependence of CDI for $rCa_v1.3_{scg}$ (○), $rCa_v1.3_L$ (●), S244G (▼), A2075V (△) and double mutant S244G/A2075V (▽). r_{50}, fraction of peak current remaining at the end of 50-ms depolarizations to the indicated test potentials. I_{Ba} measured under the same conditions is indicated for some of the constructs (same symbols, dashed line). Inset: F-values (means ± SE) were defined as the maximal difference between r_{50} values of I_{Ba} and I_{Ca} observed within the investigated voltage range (at -19 mV for all constructs). F-values of all constructs were significantly different from $rCa_v1.3_{scg}$ (one-way ANOVA with Bonferroni post-test) and from $rCa_v1.3_L$, with the exception of S244G/A2075V which was not different from $rCa_v1.3_L$.

diminishing opening (i.e., increasing $V_{0.5}$) could enhance CDI_{max}. However, with increasing $V_{0.5}$ also the fraction of channels in the inactivated mode at steady-state (F_{CDI}) [24] would decrease, due to diminished Ca^{2+} entry to drive CDI. This would result in a bell-shaped relationship between relative changes in $V_{0.5}$ and observed CDI.[24] However, mutations that strongly suppress maximum Po would also reduce F_{CDI} that resulted in observed CDI values to fall below the predicted bell-shaped curve. Therefore we measured the relationship of Q_{on}-gating currents to I_{tail} as an estimate for changes in maximum Po.[9,24] We found no changes for S244G but a strong reduction of maximal Po for A2075V. Accordingly, the increase in CDI induced by S244G can be explained by the more positive $V_{0.5}$ in the absence of changes in Po. In contrast, diminished CDI of A2075V must be determined by its lower maximal Po. Moreover, A2075V is known to decrease the affinity of the C-terminal regulatory domain for the apo-calmodulin binding site on the channel[11] which must also be regarded as a strong inhibitory factor for CDI.

Table 2. Inactivation time constants of rCa$_v$1.3 α_1-subunit mutations

	50 ms (I_{50}/I)	τ_{fast} (ms)	% τ_{fast}	τ_{slow} (ms)	n
Ca$_v$1.3 constructs					
rCa$_v$1.3$_{scg}$	0.36 ± 0.03	13.54 ± 1.05	64.37 ± 2.41	372.7 ± 41.7	12
rCa$_v$1.3$_L$	0.65 ± 0.03^{aaa}	92.94 ± 8.67^{aaa}	63.98 ± 2.50	405.1 ± 27.0	17
rCa$_v$1.3$_{scg}$ constructs					
7M2K	0.35 ± 0.02	13.43 ± 2.32	62.84 ± 3.81	313.4 ± 63.7	6
S244G	0.24 ± 0.03^{a}	9.646 ± 0.90^{a}	74.79 ± 2.27^{a}	315.9 ± 54.7	6
V11074A	0.31 ± 0.02	10.51 ± 0.61	67.09 ± 2.68	388.7 ± 58.8	7
A2075V	0.74 ± 0.03^{aaa}	110.5 ± 15.08^{aaa}	42.37 ± 2.78^{aaa}	529.6 ± 53.4^{a}	12
S244G/A2075V	0.59 ± 0.03^{aaa}	77.64 ± 10.23^{aaa}	61.36 ± 3.99	346.1 ± 31.6	16
V1104A/A2075V	0.70 ± 0.06	120.0 ± 9.49	43.08 ± 4.87	541.2 ± 119.7	6
7M2K/S244G/A2075V	0.66 ± 0.03	77.84 ± 12.29	55.85 ± 6.34	426.8 ± 38.0	6
S244G/V1104A/A2075V	0.62 ± 0.03	73.57 ± 9.49	54.94 ± 3.84	390.8 ± 39.2	9
S244G/V1104A/ex31A/A2075V	0.63 ± 0.06	75.09 ± 27.81	53.63 ± 5.73	413.9 ± 100.6	6
7M2KS244G/V1104A/ex31A/A2075V	0.64 ± 0.04	84.90 ± 14.75	65.23 ± 7.05	375.3 ± 22.5	3

Time constants for the fast (τ_{fast}) and slow (τ_{slow}) component of inactivation during 2.5 sec depolarizations to V_{max} were obtained by nonlinear curve-fitting of the experimental data to a double exponential function; % τ_{fast}, contribution of the fast component; a non-inactivating component was < 10% in all experiments and is therefore not shown.

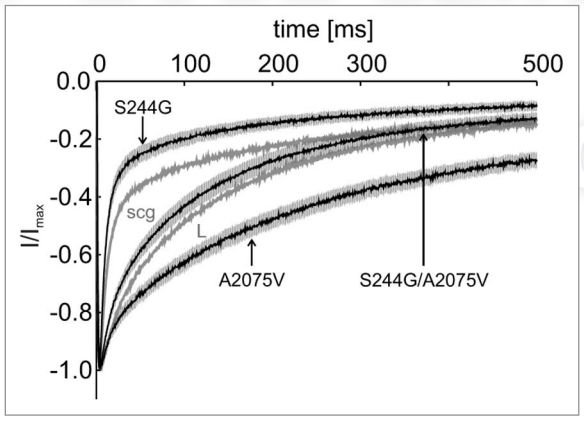

Figure 4. I_{Ca} inactivation of rCa$_v$1.3$_{scg}$ mutants. I_{Ca} inactivation of rCa$_v$1.3$_{scg}$ mutants during the first 500 ms of a 2.5 sec test pulse to V_{max}. Mutants S244G, A2075V and S244G/A2075V are illustrated. Data are shown as means (black line) with SE (gray). Inactivation time courses of rCa$_v$1.3$_L$ and rCa$_v$1.3$_{scg}$ (taken from **Fig. 1B**) are shown for comparison (light gray). Inactivation parameters are given in **Table 2**.

Our data also revealed a small but significant effect of an N-terminal sequence comprising a poly-methionine stretch followed by two lysine residues, which is not present in the rCa$_v$1.3$_{scg}$ construct. The first methionine must comprise the transcriptional start site. It is unlikely that methionine aminopeptidase removes this and subsequent methionines, because methionine residues in the second position do not support efficient cleavage.[36] It is therefore likely, that this polymethionine stretch (and the two adjacent lysine residues), which is conserved across species (e.g., mouse, human, cattle, rabbit) is present in Ca$_v$1.3 α_1-subunits and contributes to the more positive activation voltage range of rCa$_v$1.3$_L$.

We conclude that rCa$_v$1.3$_{scg}$, should not be regarded as contributor to the previously described functional heterogeneity of Ca$_v$1.3 channels as long as no unequivocal bioinformatic and biochemical evidence indicates significant expression in scg neurons or other tissues. Note that at present no evidence exists for any species differences with regard to Ca$_v$1.3 channel gating. As Ca$_v$1.3 channels are currently a promising target for drug discovery to develop neuroprotective agents in Parkinson disease,[3,37] the complex stabilization of gating properties by opposite effects of two single amino acid changes should be taken into account when interpreting previous studies employing rCa$_v$1.3$_{scg}$ α_1 constructs on the modulation of channel currents by protein interactions,[16,38] enzymes,[39] or mutations.[24]

Methods

RNA preparation. Five male Sprague-Dawley rats (10–11 weeks old) were euthanized by carbon dioxide inhalation in a saturated chamber in accordance with established welfare guidelines. The superior cervical ganglia (scg) were excised and stored in liquid nitrogen immediately. Total RNA was purified from pooled tissue using the Qiagen RNeasy Lipid Tissue Kit according to manufacturer's protocol. RNA concentration was measured using Nanodrop (NanoDrop 1000 Spectrophotometer, Thermo Scientific), and RNA quality was evaluated via separation of 28S and 18S rRNA bands on a denaturing agarose gel. One microgram of total RNA was reverse transcribed at 55°C (RevertAid^{TM} Premium First Strand cDNA Synthesis Kit, Fermentas) using random hexamer primers in a reaction volume of 20 µl. The concentration of the cDNA yielded was referred to in RNA equivalents, i.e., 1 µl of reverse transcription reaction (cDNA) was equivalent to 50 ng of RNA.

Transcript scanning and restriction analysis. PCR reactions were performed with Pfu DNA Polymerase (EP0501, Fermentas)

and 50 ng RNA equivalent from independent reverse transcriptions (95°C for 2 min, 30 cycles of 95°C for 30 sec, 58°C for 30 sec, 72°C for 1 min 15 sec, final elongation at 72°C for 5 min; 0.5 μM primer, 2 mM $MgSO_4$, 0.2 mM dNTP). Specific primer pairs (position (pos) 244: Fwd, 5'-GGA CTG CTG CTG CAT CCT AAT GCT-3'; Rev, 5'-GGA GCT GGG TCC TCT TCA GCT AC-3'; pos 1104: Fwd 5'-TGC ACA GAT GAG GCC AAA AGT AAC C-3'; Rev 5'-ACG GTG AAG ACC CCC GTG AA-3'; pos 2075: Fwd, 5'-GCC GTC GCT ACA CCG CAG TT-3'; Rev, 5'-CCT CTC GCC CAG GGT CTG GT-3') amplified fragments of 398 bp (pos 244), 620 bp (pos 1104) and 395 bp (pos 2075), respectively.

PCR products of independent PCR reactions, with independently generated cDNA templates, were purified by electrophoresis in 1.5% agarose gels and extracted using the NucleoSpin Kit (Macherey-Nagel) and ligated with the pJET1.2/blunt vector (Clone JET PCR Cloning Kit, Fermentas) for transformation of DH5α cells. Resulting clones were analyzed by colony PCR (95°C for 3 min, 30 cycles of 95°C for 30 sec, 60°C for 30 sec, 72°C for 45 sec, final elongation at 72°C for 5 min) using PCR Master Mix (K0171, Fermentas) primers flanking the multiple cloning site of the vector (Fwd, 5'-CGA CTC ACT ATA GGG AGA GCG GC-3', Rev, 5'-AAG AAC ATC GAT TTT CCA TGG CAG-3'). One aliquot of the PCR reaction was used as undigested control; other aliquots were used for restriction enzyme analysis. For each amino acid position analyzed two randomly chosen clones were also verified by sequencing (Eurofins MWG Operon).

For all clones restriction analysis was performed with enzymes specifically digesting $rCa_v1.3_L$ - containing residues: Hpy188III for G244, Hin6I for A1104, Alw26I for V2075. As a control about 10% of clones were additionally analyzed with enzymes specifically digesting $rCa_v1.3_{scg}$ sequence: BtsIMutI for S244, SduI for V1104, Bpu10I for A2075. Specific primers (see above) were used to generate positive control PCR fragments from cloned $rCa_v1.3_{scg}$.[39] Expected product sizes (bp) for samples were as follows: G244: a, 517; b, 217 + 152 + 63 + 50 + 35; c, 517; A1104: a, 739; b, 529 + 210; c, 739; V2075: a, 514; b, 261 + 253; c, 514. Expected digestion product sizes (bp) for controls: S244: 215 + 183; V1104: 468 + 152; A2075: 199 + 196 (**Fig. 2B**).

For direct PCR product sequencing gel extracted samples were directly sequenced (Eurofins MWG Operon) after PCR amplification from two independently generated scg cDNA templates and gel electrophoresis as described above.

Cell culture and transient expression. Human embryonic kindney cells (HEK293), stably expressing the SV40 temperature sensitive T antigen (tsA-201), were grown in Dulbecco's modified Eagle's medium (DMEM), supplemented with 10% v/v fetal calf serum (10270-106, Gibco), 2 mM L-glutamine (25030-032, Gibco), and 10 units/ml penicillin (P-3032, Sigma)/streptomycin (S-6501, Sigma), maintained at 37°C an 5% CO_2. Cells were splitted, when reached 80% confluency, using 0.05% Trypsin for cell dissociation. Passage did not exceed 20 numbers. Transient transfection was achieved by standard calcium phosphate precipitation method as described,[8]

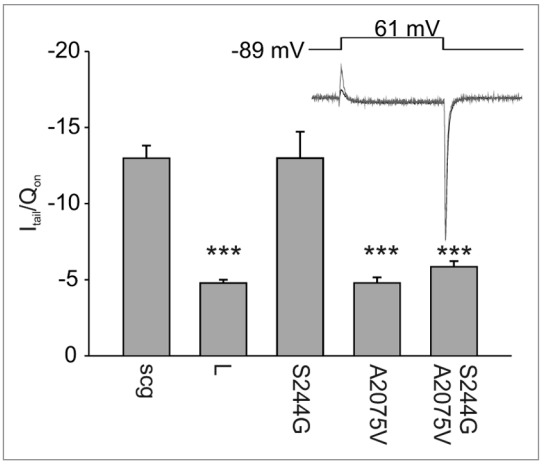

Figure 5. Changes in maximal Po of $rCa_v1.3_{scg}$ mutants. Po of $rCa_v1.3_{scg}$, $rCa_v1.3_L$ and the indicated mutants was determined from the ratios of maximal tail (ionic) current (I_{tail}) to Q_{on} (ON gating current) amplitude. Data shown are means ± SE. In comparison to $rCa_v1.3_{scg}$ Po was significantly changed for all constructs except for mutant S244G (one-way ANOVA with Bonferroni post-test). The insert shows representative current traces for $rCa_v1.3_{scg}$ (black) and $rCa_v1.3_{scg}$ mutant A2075V (gray). Currents are normalized to maximal I_{tail} amplitude. The experimental pulse protocol is shown above.

using an equimolar ratio of cDNA encoding $rCa_v1.3_{scg}$ (generously provided by Diane Lipscombe), $rCa_v1.3_L$ (generously provided by S. Seino) or the respective mutant α_1-subunits, together with auxiliary β_3 and $\alpha_2\delta$. For cell visualization 1 μg of GFP was cotransfected. For whole cell patch clamp measurements cells where then plated on 35 mm polystyrene dishes (Falcon), pretreated with poly-l-lysine.

Cloning of $Ca_v1.3$ α_1-subunit constructs. Mutations 7M2K and A2075V were introduced into $rCa_v1.3_{scg}$ by PCR using Pfu polymerase (EP0501, Fermentas). Cloning of the $rCa_v1.3_{scg}$ mutants S244G and V1104A as well as exchange of exon 31a was performed by exchange of regions of interest between $rCa_v1.3_L$ and $rCa_v1.3_{scg}$ or $rCa_v1.3_{scg}$ A2075V. After restriction enzyme digestion fragments of $rCa_v1.3_L$ (carrying $rCa_v1.3_L$ specific-sequence) were incorporated into $rCa_v1.3_{scg}$ or $rCa_v1.3_{scg}$ A2075V to replace the $Ca_v1.3_{scg}$-specific sequence. Enzyme combinations were as follows: S244G: BsiWI, BamHI; V1104A: BamHI, BglII, KpnI; ex 31A: EcoRV, BamHI. $rCa_v1.3_L$, $rCa_v1.3_{scg}$ and all mutations were verified by sequencing (Eurofins MWG Operon).

Electrophysiology. For whole cell patch clamp recordings borosilicate glass electrodes where pulled (micropipette puller, Sutter Instruments) and fire polished (microforge, Narishinge MF-830), having a final resistance of 2–5 MΩ. Cells were recorded in whole-cell configuration using an Axopatch 200B amplifier (Axon instruments). Data were digitized (Digitizer 1322A, Axon Instruments) and analysis was performed by pClamp 10.2 software (Axon Instruments). The recording solutions contained in mM: pipette solution: 135 CsCl, 10 HEPES, 10 Cs-EGTA, 1 $MgCl_2$ adjusted to pH 7.4 with CsOH; bath solution: 15 $CaCl_2$ or $BaCl_2$, 10 HEPES, 150 choline-Cl and 1 $MgCl_2$, adjusted to pH 7.4 with CsOH. Cells were held at a

holding potential of -80 mV, before current-voltage (I - V) relationships were obtained by applying 10 ms square pulse protocol to various test potentials. For leak subtraction a P/4 protocol was used. I - V curves were fitted to the equation $I = G_{max} (V - V_{rev})/\{1 + \exp[(V - V_{0.5})/k_{act}]\}$, where V_{rev} is the extrapolated reversal potential, V is the test potential, I is the peak current amplitude, G_{max} is the maximum slope conductance, $V_{0.5}$ is the half maximal activation voltage and k_{act} is the slope factor. Inactivation was determined by a 2.5 sec long pulse to V_{max}, and fit by standard double exponential decay, via Graph Pad Prism 5 (GraphPad Software Inc.). Voltage dependence of the inactivation time course was determined by a 300 ms long step protocol to various test potentials.

As an estimate for the maximal channel open probability we compared the amplitude of ON-gating currents (Q_{on}) with ionic tail currents (I_{tail}) during 10 ms test pulses to 61 mV and repolarization to -80 mV.

Statistics. Data analysis was performed by Clampfit 10.2 (Axon Instruments) and Sigma Plot 11 (Systat Software Inc.). All data are represented as mean ± SE. For statistical analysis one-way ANOVA with Bonferroni post-test or Student's t-test was performed using Graph Pad Prism 5.1 software (GraphPad Software Inc.). Significance level was set to α error lower than $p < 0.05$.

Disclosure of Potential Conflicts of Interest

No potential conflicts of interest were disclosed.

Acknowledgments

We thank Alexandra Koschak, Diane Lipscombe and Petronel Tuluc for helpful discussions; Florian Hechenblaikner for sharing preliminary data on mouse $Ca_v1.3$ constructs; Diane Lipscombe for supplying the $rCa_v1.3_{scg}$ construct; Susumo Seino for the $rCa_v1.3_L$ construct, Ed Perez-Reyes for β_3-subunit cDNA; Gospava Stojanovic, Jennifer Müller and Germana Gratl for competent technical assistance. This work was supported by the Austrian Science Fund (P-20670, W1101-B12) and the University of Innsbruck.

References

1. Namkung Y, Skrypnyk N, Jeong MJ, Lee T, Lee MS, Kim HL, et al. Requirement for the L-type Ca^{2+} channel α_1D -subunit in postnatal pancreatic beta cell generation. J Clin Invest 2001; 108:1015-22; PMID:11581302.
2. Platzer J, Engel J, Schrott-Fischer A, Stephan K, Bova S, Chen H, et al. Congenital deafness and sinoatrial node dysfunction in mice lacking class D L-type Ca^{2+} channels. Cell 2000; 102:89-97; PMID:10929716; http://dx.doi.org/10.1016/S0092-8674(00)00013-1.
3. Striessnig J, Koschak A. Exploring the function and pharmacotherapeutic potential of voltage-gated Ca^{2+} channels with gene knockout models. Channels (Austin) 2008; 2:233-51; PMID:18719397; http://dx.doi.org/10.4161/chan.2.4.5847.
4. Baig SM, Koschak A, Lieb A, Gebhart M, Dafinger C, Nürnberg G, et al. Loss of $Ca_v1.3$ (CACNA1D) function in a human channelopathy with bradycardia and congenital deafness. Nat Neurosci 2011; 14:77-84; PMID:21131953; http://dx.doi.org/10.1038/nn.2694.
5. Mahapatra S, Marcantoni A, Vandael DH, Striessnig J, Carbone E. Are $Ca_v1.3$ pacemaker channels in chromaffin cells? Possible bias from resting cell conditions and DHP blockers usage. Channels (Austin) 2011; 5:219-24; PMID:21406973; http://dx.doi.org/10.4161/chan.5.3.15271.
6. Brandt A, Striessnig J, Moser T. $Ca_V1.3$ channels are essential for development and presynaptic activity of cochlear inner hair cells. J Neurosci 2003; 23:10832-40; PMID:14645476.
7. Michna M, Knirsch M, Hoda JC, Muenkner S, Langer P, Platzer J, et al. $Ca_v1.3$ α_1D Ca^{2+} currents in neonatal outer hair cells of mice. J Physiol 2003; 553:747-58; PMID:14514878; http://dx.doi.org/10.1113/jphysiol.2003.053256.
8. Bock G, Gebhart M, Scharinger A, Jangsangthong W, Busquet P, Poggiani C, et al. Functional properties of a newly identified C-terminal splice variant of $Ca_v1.3$ L-type Ca^{2+} channels. J Biol Chem 2011; 286:42736-48; PMID:21998310; http://dx.doi.org/10.1074/jbc.M111.269951.
9. Singh A, Gebhart M, Fritsch R, Sinnegger-Brauns MJ, Poggiani C, Hoda JC, et al. Modulation of voltage- and Ca^{2+}-dependent gating of $Ca_V1.3$ L-type calcium channels by alternative splicing of a C-terminal regulatory domain. J Biol Chem 2008; 283:20733-44; PMID:18482979; http://dx.doi.org/10.1074/jbc.M802254200.
10. Huang H, Tan BZ, Shen Y, Tao J, Jiang F, Sung YY, et al. RNA editing of the IQ domain in $Ca_v1.3$ channels modulates their Ca^{2+}-dependent inactivation. Neuron 2012; 73:304-16; PMID:22284185; http://dx.doi.org/10.1016/j.neuron.2011.11.022.
11. Liu X, Yang PS, Yang W, Yue DT. Enzyme-inhibitor-like tuning of Ca^{2+} channel connectivity with calmodulin. Nature 2010; 463:968-72; PMID:20139964; http://dx.doi.org/10.1038/nature08766.
12. Tan GM, Yu D, Wang J, Soong TW. Alternative splicing at C terminus of $Ca_V1.4$ calcium channel modulates calcium-dependent inactivation, activation potential and current density. J Biol Chem 2012; 287:832-47; PMID:22069316; http://dx.doi.org/10.1074/jbc.M111.268722.
13. Koschak A. Impact of gating modulation in $Ca_V1.3$ L-type calcium channels. Channels (Austin) 2010; 4:523-5; PMID:21150316; http://dx.doi.org/10.4161/chan.4.6.12872.
14. Minor DL Jr, Findeisen F. Progress in the structural understanding of voltage-gated calcium channel Ca_V function and modulation. Channels (Austin) 2010; 4:459-74; PMID:21139419.
15. Xu W, Lipscombe D. Neuronal $Ca_V1.3\alpha_1$ L-type channels activate at relatively hyperpolarized membrane potentials and are incompletely inhibited by dihydropyridines. J Neurosci 2001; 21:5944-51; PMID:11487617.
16. Yang PS, Alseikhan BA, Hiel H, Grant L, Mori MX, Yang W, et al. Switching of Ca^{2+}-dependent inactivation of $Ca_v1.3$ channels by calcium binding proteins of auditory hair cells. J Neurosci 2006; 26:10677-89; PMID:17050707; http://dx.doi.org/10.1523/JNEUROSCI.3236-06.2006.
17. Helton TD, Xu W, Lipscombe D. Neuronal L-type calcium channels open quickly and are inhibited slowly. J Neurosci 2005; 25:10247-51; PMID:16267232; http://dx.doi.org/10.1523/JNEUROSCI.1089-05.2005.
18. Shen Y, Yu D, Hiel H, Liao P, Yue DT, Fuchs PA, et al. Alternative splicing of the $Ca_v1.3$ channel IQ domain, a molecular switch for Ca^{2+}-dependent inactivation within auditory hair cells. J Neurosci 2006; 26:10690-9; PMID:17050708; http://dx.doi.org/10.1523/JNEUROSCI.2093-06.2006.
19. Huang H, Tan BZ, Shen Y, Tao J, Jiang F, Sung YY, et al. RNA editing of the IQ domain in $Ca_v1.3$ channels modulates their Ca^{2+}-dependent inactivation. Neuron 2012; 73:304-16; PMID:22284185; http://dx.doi.org/10.1016/j.neuron.2011.11.022.
20. Tadross MR, Dick IE, Yue DT. Mechanism of local and global Ca^{2+} sensing by calmodulin in complex with a Ca^{2+} channel. Cell 2008; 133:1228-40; PMID:18585356; http://dx.doi.org/10.1016/j.cell.2008.05.025.
21. Klugbauer N, Welling A, Specht V, Seisenberger C, Hofmann F. L-type Ca^{2+} channels of the embryonic mouse heart. Eur J Pharmacol 2002; 447:279-84; PMID:12151019; http://dx.doi.org/10.1016/S0014-2999(02)01850-2.
22. Tan BZ, Jiang F, Tan MY, Yu D, Huang H, Shen Y, et al. Functional characterization of alternative splicing in the C terminus of L-type $Ca_V1.3$ channels. J Biol Chem 2011; 286:42725-35; PMID:21998309; http://dx.doi.org/10.1074/jbc.M111.265207.
23. Tadross MR, Yue DT. Systematic mapping of the state dependence of voltage- and Ca^{2+}-dependent inactivation using simple open-channel measurements. J Gen Physiol 2010; 135:217-27; PMID:20142518; http://dx.doi.org/10.1085/jgp.200910309.
24. Tadross MR, Ben Johny M, Yue DT. Molecular endpoints of Ca^{2+}/calmodulin- and voltage-dependent inactivation of $Ca_v1.3$ channels. J Gen Physiol 2010; 135:197-215; PMID:20142517; http://dx.doi.org/10.1085/jgp.200910308.
25. Safa P, Boulter J, Hales TG. Functional properties of $Ca_v1.3$ α_1D L-type Ca^{2+} channel splice variants expressed by rat brain and neuroendocrine GH3 cells. J Biol Chem 2001; 276:38727-37; PMID:11514547; http://dx.doi.org/10.1074/jbc.M103724200.
26. Griessmeier K, Cuny H, Rötzer K, Griesbeck O, Harz H, Biel M, et al. Calmodulin is a functional regulator of $Ca_v1.4$ L-type Ca^{2+} channels. J Biol Chem 2009; 284:29809-16; PMID:19717559; http://dx.doi.org/10.1074/jbc.M109.048082.
27. Wahl-Schott C, Baumann L, Cuny H, Eckert C, Griessmeier K, Biel M. Switching off calcium-dependent inactivation in L-type calcium channels by an autoinhibitory domain. Proc Natl Acad Sci USA 2006; 103:15657-62; PMID:17028172; http://dx.doi.org/10.1073/pnas.0604621103.
28. Singh A, Hamedinger D, Hoda JC, Gebhart M, Koschak A, Romanin C, et al. C-terminal modulator controls Ca^{2+}-dependent gating of $Ca_v1.4$ L-type Ca^{2+} channels. Nat Neurosci 2006; 9:1108-16; PMID:16921373; http://dx.doi.org/10.1038/nn1751.

29. Hulme JT, Westenbroek RE, Scheuer T, Catterall WA. Phosphorylation of serine 1928 in the distal C-terminal domain of cardiac $Ca_V1.2$ channels during beta1-adrenergic regulation. Proc Natl Acad Sci USA 2006; 103:16574-9; PMID:17053072; http://dx.doi.org/10.1073/pnas.0607294103.
30. Fu Y, Westenbroek RE, Yu FH, Clark JP, 3rd, Marshall MR, Scheuer T, et al. Deletion of the distal C terminus of $Ca_V1.2$ channels leads to loss of beta-adrenergic regulation and heart failure in vivo. J Biol Chem 2011; 286:12617-26; PMID:21216955; http://dx.doi.org/10.1074/jbc.M110.175307.
31. Danecek P, Nellåker C, McIntyre RE, Buendia-Buendia JE, Bumpstead S, Ponting CP, et al. High levels of RNA-editing site conservation amongst 15 laboratory mouse strains. Genome Biol 2012; 13:26; PMID:22524474; http://dx.doi.org/10.1186/gb-2012-13-4-r26.
32. Gallo A, Thomson E, Brindle J, O'Connell MA, Keegan LP. Micro-processing events in mRNAs identified by DHPLC analysis. Nucleic Acids Res 2002; 30:3945-53; PMID:12235378; http://dx.doi.org/10.1093/nar/gkf516.
33. Payandeh J, Scheuer T, Zheng N, Catterall WA. The crystal structure of a voltage-gated sodium channel. Nature 2011; 475:353-8; PMID:21743477; http://dx.doi.org/10.1038/nature10238.
34. Hoda JC, Zaghetto F, Koschak A, Striessnig J. Congenital stationary night blindness type 2 mutations S229P, G369D, L1068P and W1440X alter channel gating or functional expression of $Ca_V1.4$ L-type Ca^{2+} channels. J Neurosci 2005; 25:252-9; PMID:15634789; http://dx.doi.org/10.1523/JNEUROSCI.3054-04.2005.
35. Tottene A, Pivotto F, Fellin T, Cesetti T, van den Maagdenberg AM, Pietrobon D. Specific kinetic alterations of human $Ca_V2.1$ calcium channels produced by mutation S218L causing familial hemiplegic migraine and delayed cerebral edema and coma after minor head trauma. J Biol Chem 2005; 280:17678-86; PMID:15743764; http://dx.doi.org/10.1074/jbc.M501110200.
36. Frottin F, Martinez A, Peynot P, Mitra S, Holz RC, Giglione C, et al. The proteomics of N-terminal methionine cleavage. Mol Cell Proteomics 2006; 5:2336-49; PMID:16963780; http://dx.doi.org/10.1074/mcp.M600225-MCP200.
37. Surmeier DJ, Guzman JN, Sanchez-Padilla J. Calcium, cellular aging and selective neuronal vulnerability in Parkinson's disease. Cell Calcium 2010; 47:175-82; PMID:20053445; http://dx.doi.org/10.1016/j.ceca.2009.12.003.
38. Calin-Jageman I, Yu K, Hall RA, Mei L, Lee A. Erbin enhances voltage-dependent facilitation of $Ca_V1.3$ Ca^{2+} channels through relief of an autoinhibitory domain in the $Ca_V1.3$ α_1-subunit. J Neurosci 2007; 27:1374-85; PMID:17287512; http://dx.doi.org/10.1523/JNEUROSCI.5191-06.2007.
39. Gao L, Blair LA, Salinas GD, Needleman LA, Marshall J. Insulin-like growth factor-1 modulation of $Ca_V1.3$ calcium channels depends on Ca^{2+} release from IP3-sensitive stores and calcium/calmodulin kinase II phosphorylation of the α_1-subunit EF hand. J Neurosci 2006; 26:6259-68; PMID:16763033; http://dx.doi.org/10.1523/JNEUROSCI.0481-06.2006.